

# RHEOLOGICAL BEHAVIOR OF FUGITIVE ORGANIC INKS FOR DIRECT-WRITE ASSEMBLY

DANIEL THERRIAULT<sup>\*1</sup>, SCOTT R. WHITE<sup>2</sup> AND JENNIFER A. LEWIS<sup>3</sup>

<sup>1</sup> Mechanical Engineering Department, Center for Applied Research on Polymers and Composites (CREPEC), École Polytechnique de Montréal, Montréal, Québec H3C 3A7, Canada

<sup>2</sup> Beckman Institute for Advanced Science and Technology, Autonomic Materials Systems Group, Aerospace Engineering, University of Illinois at Urbana-Champaign, 306 Talbot Lab, 104 S. Wright St., Urbana, IL 61801, USA

<sup>3</sup> Materials Science and Engineering Department, Frederick Seitz Materials Research Laboratory, NSF Center for Directed Assembly of Nanostructures, University of Illinois at Urbana-Champaign, 212d Ceramics Bldg., 1304 W. Green St., Urbana, IL 61801, USA

\*E-mail: daniel.therriault@polymtl.ca

Fax: x1.514.340.4176

Received: 21.7.2006, Final version: 15.9.2006

## ABSTRACT:

The rheological behavior of a fugitive organic ink tailored for direct-write assembly of 3D microfluidic devices is investigated. Rheological experiments are carried out to probe the shear storage and loss moduli as well as the complex viscosity as a function of varying temperature, frequency and stress amplitude. Master curves of these functions are assembled using time-temperature superposition. The fugitive ink, comprised of two organic phases, possesses an equilibrium shear elastic modulus nearly two orders of magnitude higher than that of a commercial reference ink at room temperature and a peak in the relaxation spectrum nearly six orders of magnitude longer in time scale. The self-supporting nature of extruded ink filaments is characterized by direct video imaging. Comparison of the experimentally observed behavior to numerical predictions based on Euler-Bernoulli viscoelastic beam analysis yield excellent agreement for slender filaments.

## ZUSAMMENFASSUNG:

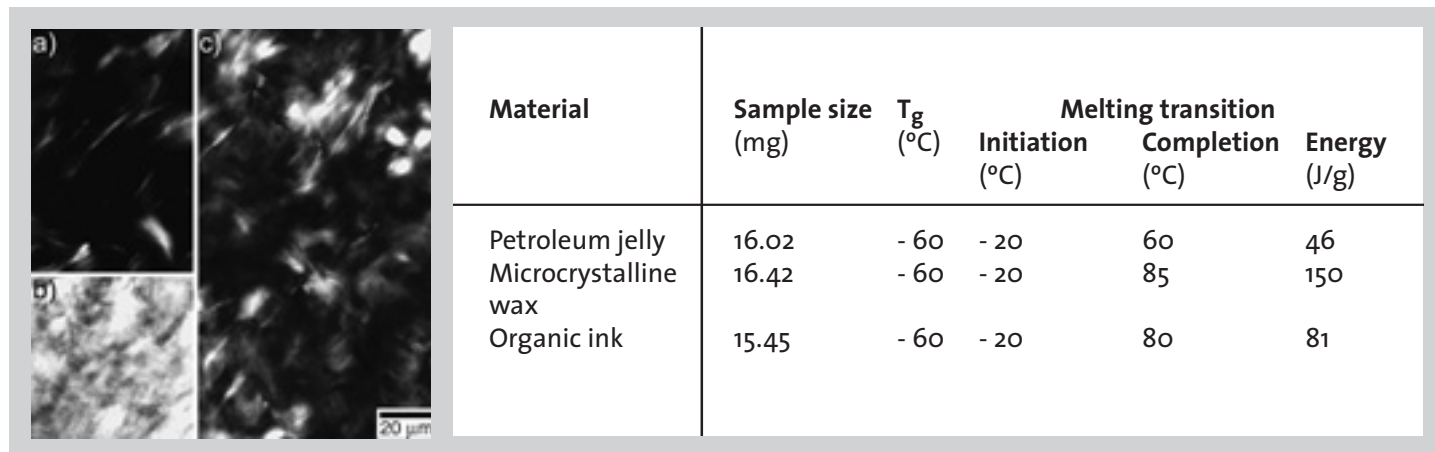
Das rheologische Verhalten einer flüchtigen organischen Tinte für die Herstellung dreidimensionaler mikro-strömungstechnischer Apparate mittels Direkt-Schreibens wurde untersucht. Über rheologische Messungen wurden Speicher- und Verlustmodul sowie die komplexe Viskosität als Funktion verschiedener Temperaturen, Frequenzen und Schubspannungsamplituden bestimmt. Die Masterkurven für diese Funktionen wurden mit Hilfe der Zeit-Temperatur-Superposition zusammengestellt. Die flüchtige Tinte, die ein Gemisch zweier organischer Komponenten ist, weist bei Raumtemperatur ein um ungefähr zwei Dekaden größeres Gleichgewichtsspeichermodul als das einer kommerziell erworbenen Referenztinte auf und das Maximum des Relaxationsspektrums ist um sechs Dekaden länger in der Zeit. Die selbsttragende Natur extrudierter Tintenfäden wurde mittels digitaler Bildanalyse charakterisiert. Die experimentellen Beobachtungen stimmen mit numerischen Berechnungen nach dem viskoelastischen Balkenmodell von Euler-Bernoulli für dünne Stränge sehr gut überein.

## RÉSUMÉ:

Le comportement rhéologique d'une encre fugitive organique utilisée pour l'écriture directe d'appareils microfluidiques tridimensionnels est étudié. Des expériences rhéologiques ont été réalisées pour quantifier les modules élastique et de perte en cisaillement ainsi que la viscosité complexe de l'encre en fonction de différentes températures, fréquences et amplitudes de contrainte. Les courbes maîtresses de ces fonctions ont été assemblées à l'aide de la superposition temps-température. L'encre fugitive, mélange de deux composants organiques, possède à température ambiante un module élastique de cisaillement à l'équilibre environ deux décades supérieur de celui d'une encre commerciale utilisée comme référence et le sommet de son spectre de relaxation est six décades plus long dans le temps. Le comportement auto-supporteur de filaments d'encres extrudés a été caractérisé par l'analyse d'images numérisées. La comparaison entre les résultats expérimentaux observés et les prédictions numériques obtenues à l'aide d'un modèle de poutre viscoélastique Euler-Bernoulli donne un excellent accord pour un filament élancé.

**KEY WORDS:** Direct-write, viscoelastic material, organic ink, structural behavior, microfabrication

© Appl. Rheol. 17 (2007) 10112-1 – 10112-8



## 1 INTRODUCTION

The recent progress in advanced fabrication technologies has enabled the creation of microfluidic devices with high commercial potential in biomedicine [1], chemistry [2], environmental testing [3], and autonomic materials [4]. Fluid transport within microchannels is dominated by laminar flow and diffusive mixing [5]. Although such devices are readily constructed in two-dimensions (2D) by conventional approaches such as lithographic techniques, the construction of complex three-dimensional (3D) microfluidic networks is critical for future applications requiring multiplexing and efficient mixing.

Direct-write assembly enables the construction of complex 3D structures in a layerwise deposition scheme without the need for expensive tooling, dies, or lithographic masks [6]. Recently, we have demonstrated that 3D microvascular networks embedded within a polymer matrix [5, 7] can be fabricated by robotically depositing [8] a fugitive ink in the form of a self-supporting scaffold structure. Subsequent infiltration of the fugitive scaffold with a thermosetting resin followed by curing and scaffold removal yields an embedded network of smooth cylindrical channels with pervasive connectivity [5]. Successful network fabrication requires a fugitive ink with highly tailored viscoelastic properties. First, the ink must flow through a fine deposition nozzle under high shear, yet be self-supporting once deposited. Second, the fugitive ink scaffold must maintain its shape during resin infiltration and subsequent polymerization, yet liquefy at moderate temperatures to facilitate its removal from the templated matrix.

Here we systematically study the rheological properties and structural behavior of a fugitive organic ink used to construct complex 3D microvascular networks [7]. We begin with characterization of material behavior using spectroscopy, microscopy and thermal analysis and proceed to detailed studies of ink rheology. From this data the linear viscoelastic regime is identified along with master curves of several vis-

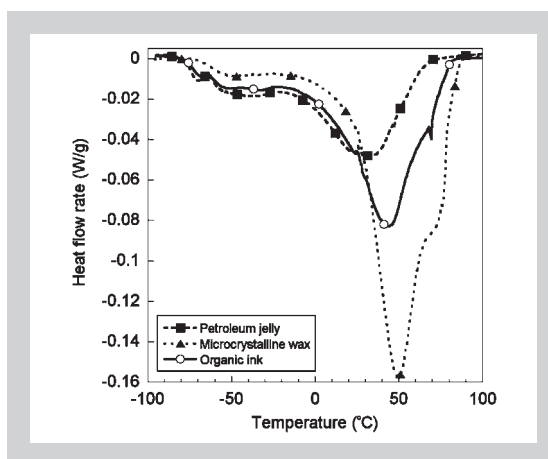


Figure 1 (left above): Polarized (crossed polarizers) optical microscope images of a) petroleum jelly, b) microcrystalline wax, and c) organic ink (1.5:1 blend a:b).

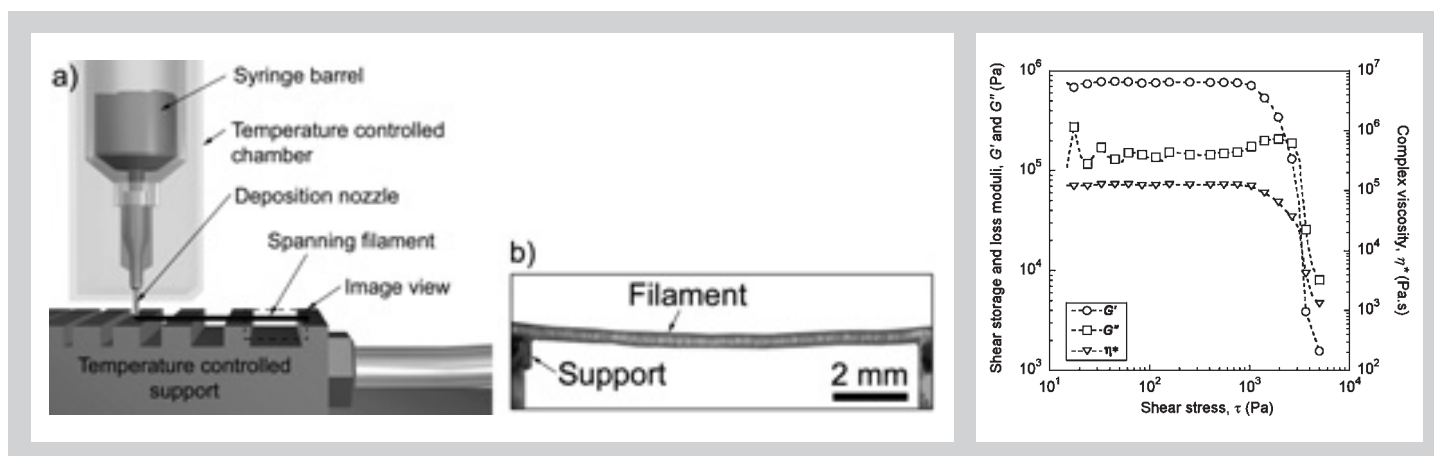
Figure 2: Differential scanning calorimetry results of organic ink and its constituents during dynamic scanning at  $2.5^\circ\text{C min}^{-1}$ .

Table 1: Differential scanning calorimetry results.

coelastic functions. A simple structural model of the time-dependent deformation of ink filaments is then developed and compared to experimental observations.

## 2 MATERIALS AND EXPERIMENTAL METHODS

An organic ink composed of a mixture of low and high molecular weight constituents was prepared by first melting ( $\sim 75^\circ\text{C}$ ) the low molecular weight constituent ( $M_w = 840$  g/mol, Vaseline<sup>®</sup> petroleum jelly, Chesebrough-Pond's, Ladson, SC, USA) and then adding 40 wt% microcrystalline wax ( $M_w = 1450$  g/mol, SP 18, Strahl & Pitsch Inc., West Babylon, NY, USA) while homogenizing by magnetic stirring for 20 min. The molecular weight of the binary organic ink (bimodal distribution with  $M_w = 1050$  g/mol) and its constituents were determined by gel permeation chromatography (GPC) (TDA Model 300, Viscotek, Houston, TX, USA). The GPC apparatus was calibrated using polystyrene standards for low molecular-weight measurements. The microcrystalline wax is composed of hydrocarbon chains that undergo crystallization upon cooling from the molten state [9]. Optical images of the organic ink and its constituents acquired using crossed polarizers (Figure 1) reveal the presence of crystalline (light) and amorphous (dark) phas-



Ink	L/d	L (mm)	d (mm)	Platform velocity (mm/s)	Deposition pressure (kPa)
Organic	10.7	11.50	1.07	6.0	358
	14.8	6.52	0.44	2.0	646
	26.1	11.50	0.44	2.0	646
Commercial	10.7	11.50	1.07	6.0	103
	14.8	6.52	0.44	6.0	247

Figure 3 (left): Self-supporting ink filament deformation experiments. a) Experimental setup showing image view. b) Representative optical image for organic ink ( $L/d = 26.1$ ) at  $t \sim 25$  min and  $T = 20^\circ\text{C}$ .

Figure 4: Rheological behavior of organic ink as a function of applied shear stress amplitude. ( $T = 25^\circ\text{C}$ ,  $f = 1$  Hz).

Table 2: Experimental conditions for self-supporting filament deformation experiments.

es. The extent of crystallinity as measured by image analysis was  $\sim 25$ ,  $\sim 40$ , and  $\sim 6.6\%$  for the organic ink, microcrystalline wax and petroleum jelly, respectively.

Differential scanning calorimetry (DSC821e, Mettler Toledo, Columbus, OH, USA) experiments were performed on the organic ink and its constituents over a temperature range from  $-100$  to  $100^\circ\text{C}$  while heating at  $2.5^\circ\text{C}/\text{min}$ . These data are shown in Figure 2 and summarized in Table 1. The three samples feature a glass transition temperature,  $T_g$ ,  $\sim -60^\circ\text{C}$  and a primary melting transition located between  $-20^\circ\text{C}$  and either  $60^\circ\text{C}$  (petroleum jelly),  $85^\circ\text{C}$  (microcrystalline wax), or  $80^\circ\text{C}$  (organic ink). The microcrystalline wax exhibits the largest normalized energy (i.e.  $\sim 150$  J/g) during the melting transition due to the high degree of crystallinity for this material. The extent of crystallinity was calculated for each material by comparing the measured energy of the melt transition to the heat of fusion of theoretically 100% crystalline polyethylene ( $H_f = 294$  J/g [10]). The degree of crystallinity from DSC analysis was found to be 28, 51, and 16% for the organic ink, microcrystalline wax and petroleum jelly, respectively. These values are consistent with, albeit slightly higher than, those obtained from optical image analysis.

To characterize the viscoelastic behavior of the organic ink, oscillatory shear experiments were carried out using a controlled stress rheometer (Bohlin CVOR-200 apparatus, Cranbury, NJ, USA) fitted with a concentric cylinder geometry (C-14 cell). An appropriate volume (3

ml) of ink was first melted at  $\sim 75^\circ\text{C}$ , poured into the measurement cell, and then cooled to the desired temperature,  $T$ , using a circulating temperature bath (Model 9110, Polyscience, Chicago, IL, USA). After an equilibration period under quiescent conditions ( $\sim 15$  min), the sample was sheared by rotating the inner cylinder at a prescribed rate and amplitude (i.e. angle of rotation) while measuring the torque. These data were then used to compute the complex shear modulus ( $G^* = G' + iG''$ , where  $G'$  shear storage modulus,  $G''$  shear loss modulus) and the complex viscosity ( $\eta^* = G^*/i\omega$ ;  $\eta^* = \eta' + i\eta''$ , where  $\eta'$  dynamic viscosity,  $\eta''$  dynamic rigidity,  $\omega$  is angular frequency).

The time-dependent deflection of filaments was measured by optical imaging using the experimental setup illustrated in Figure 3a. Prior to initiating the experiment, the temperature is allowed to equilibrate ( $\sim 15$  min) to ensure a uniform ink temperature within the deposition nozzle (barrel diameter = 4.6 mm, EFD Inc., East Providence, RI, USA) and the support structure, both of which were maintained and controlled by a recirculator bath (Model F25-MC, Allentown, PA, USA). Isothermal conditions were confirmed by embedded thermocouple measurements within the filament. An ink filament (diameter,  $d$ ) is then deposited using a robotic deposition apparatus (Model JL2000, Robocasting Enterprises, Inc., Albuquerque, NM, USA) over a specific spanning distance,  $L$ , at  $20^\circ\text{C}$ . The deposition parameters used for the organic and commercial inks studied are listed in Table 2. The aspect ratios,  $L/d$ , studied ranged from 10.7 to 26.1, however the formation of long, slender filaments ( $L/d = 26.1$ ) comprised of the commercial ink was not possible due to rupture and/or immediate slumping of the filament. Immediately after deposition, the ink filaments (side view) are imaged with a video camera through a telescopic lens. The digital images are stored at 30 frames/sec ( $\Delta t = 0.033$  s) with a resolution of  $720 \cdot 480$  pixels (1 pixel  $\sim 15$   $\mu\text{m}$  at 5x magnification). Through

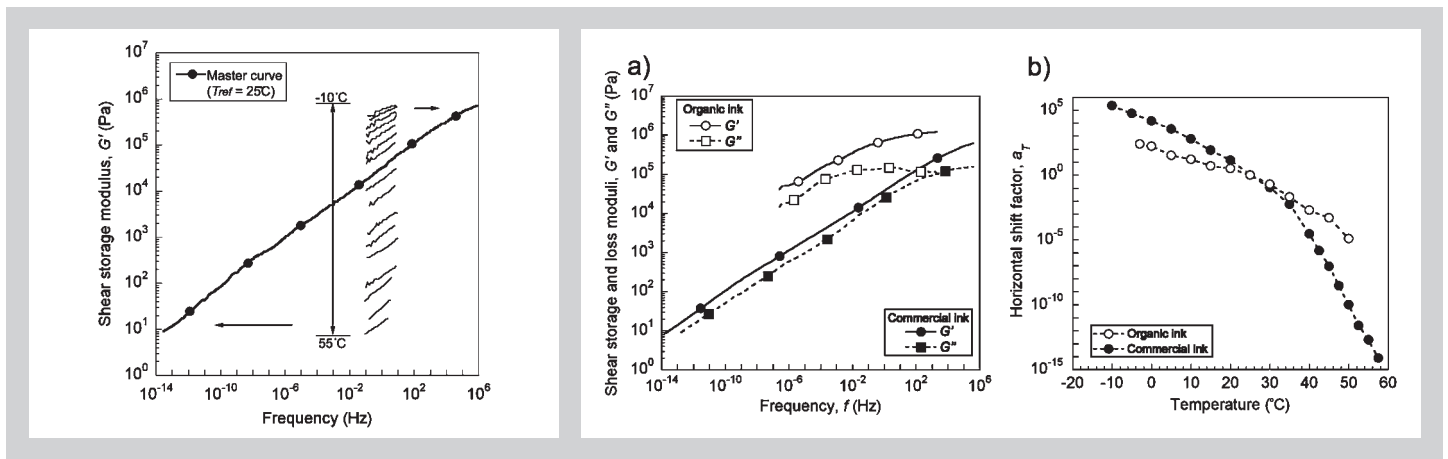


image processing, the mid-span deflection of each filament was determined as a function of time for approximately 30 time intervals equally spaced on a logarithmic scale ranging from 0.033 s to 25 – 60 min. The initial data point ( $t = 0.033$  s) is recorded when the filament first contacts the second rigid support upon exiting the nozzle.

### 3 RHEOLOGICAL BEHAVIOR OF FUGITIVE INKS

The ink elasticity and apparent shear yield stress,  $\tau_y^{app}$ , are measured by carrying out a stress sweep, in which the shear stress amplitude was gradually increased at a constant frequency,  $f$ , of 1 Hz. In the linear elastic regime ( $\tau < \tau_y^{app}$ ), the sample deforms elastically, i.e., its mechanical properties are independent of applied stress. Once the applied shear stress exceeds  $\tau_y^{app}$ , the ink microstructure is perturbed and significant flow occurs during deformation. The value of  $\tau_y^{app}$  for polymeric systems is commonly defined as the stress level where the material stiffness (e.g.  $G'$ ) reduces to 90% of the plateau value,  $G_o$  [11]. Figure 4 shows results for the dynamic shear moduli and magnitude of the complex viscosity as a function of applied stress at ambient temperature. A solid-like response is observed at low applied shear stress where the storage modulus exceeds the loss modulus by a factor of  $\sim 5$ , and the complex viscosity is constant and relatively high. The material yields at a stress level of  $\tau_y^{app} \sim 1.01$  kPa which corresponds to a shear strain,  $\gamma$ , of  $\sim 1.6 \cdot 10^{-3}$ . Above  $\tau_y^{app}$ , the stiffness and viscosity rapidly decrease and a fluid-like transition is reached at  $\tau = 2.34$  kPa ( $\gamma \sim 7.8 \times 10^{-3}$ ) when  $G'' = G'$ .

To further probe the linear viscoelastic regime, frequency sweeps were carried out from 0.1 to 10 Hz at a prescribed strain amplitude ( $\gamma = 5 \cdot 10^{-5}$  for all temperatures) well below the yield point. As a benchmark for comparison, a commercial organic material (Prussian blue paste®,

Loctite, Rocky Hill, CT, USA), which served as our original fugitive ink [5] for direct-write assembly, was also characterized. The commercial ink consists of a mixture of paraffin wax, mineral oil, and ferric ferrocyanide nanoparticles ( $\text{Fe}_4[\text{Fe}(\text{CN})_6]_3 \sim 2.2$  wt%) with a typical size of 20 - 150 nm [12]. Specifically, frequency sweeps are carried out at 12 different isothermal temperatures ranging from -3 to 50°C for the fugitive organic ink and 17 temperatures from -10 to 55°C for the commercial ink in order to construct master curves of viscoelastic functions in the frequency domain using the time-temperature superposition principle [13 - 15]. Assuming the density correction to be negligible, the amount by which each isothermal curve was shifted is temperature dependent and is defined as [13]:

$$\begin{aligned} G'(f, T_o) &= G'(fa_T, T) \\ \eta^*(f, T_o) &= \frac{\eta^*(fa_T, T)}{a_T} \end{aligned} \quad (1)$$

where  $a_T$  is the temperature shift factor and  $T_o$  is the reference temperature. Figure 5 shows the master curve construction of the shear storage modulus,  $G'$ , for the commercial ink. Using ambient conditions as the reference state ( $T_o = 25^\circ\text{C}$ ), the experimental results obtained at colder and warmer temperatures were shifted to higher and lower frequencies, respectively, to construct a master curve covering more than 10 decades in the frequency domain. The assembled master curves of  $G'$  and  $G''$  and the shift factors used in their construction for both inks are shown in Figure 6. The organic ink features a plateau value of  $G' \sim 1.2$  MPa at high frequencies ( $\sim 10^2$  Hz) and monotonically decreases with frequency below  $\sim 10^{-2}$  Hz. The commercial ink behaved similarly, but with significantly lower values across the entire spectrum of frequencies (e.g.  $G' \sim 0.52$  MPa at  $10^5$  Hz). The logarithmic values of the organic ink shift factor decreased linearly with increasing temperature over the temperature range

Figure 5 (left): Shear storage modulus master curve assembly for the commercial ink.

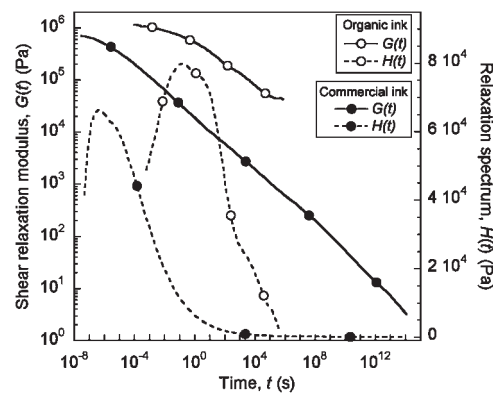
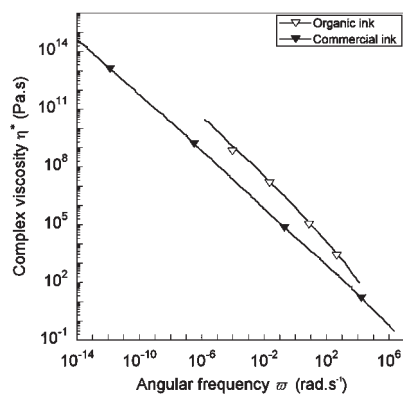
Figure 6: Results of isothermal oscillatory shear rheometry experiments.

- a) Complex shear modulus master curves,  $T_{ref} = 25^\circ\text{C}$ .
- b) Shift factors used in master curve construction.

Figure 7 (left): Complex viscosity master curves for  $T_{ref} = 25^{\circ}C$ .

Figure 8: Shear relaxation modulus (solid lines) and spectrum (dashed lines) as a function of time,  $T_{ref} = 25^{\circ}C$ .

Table 3: Parameters of power-law representation of viscosity.



Material	m (Pa·s <sup>n</sup> )	n
Organic ink	$4.62 \cdot 10^5$	0.156
Commercial ink	$2.23 \cdot 10^4$	0.262

studied while a bi-linear temperature dependence was observed for the commercial ink.

The shift factors shown in Fig. 6b are also used to assemble, via horizontal and vertical shifts, the  $\eta^*$  master curve of each ink. Viscosity,  $\eta$ , is estimated using the Cox-Merz empirical relation given by [13]

$$\eta(\dot{\gamma})|_{\dot{\gamma}=\omega} = |\eta^*(\omega)| \quad (2)$$

This relation is often used to approximate shear viscosity data of polymer solutions and melts from oscillatory shear rheometric data [13]. The master curves for both materials are shown in Figure 7. Shear-thinning behavior is readily apparent as  $\eta$  decreases linearly with increasing  $\dot{\gamma}$  in log-log coordinates. As expected for materials with a yield stress,  $\eta$  tends to infinity as  $\dot{\gamma}$  approaches zero (i.e. solid-like behavior). The absence of a low-shear rate plateau yields a power-law representation of the data [13]

$$\eta = m|\dot{\gamma}|^{n-1} \quad (3)$$

where  $m$  and  $n$  are obtained from experimental correlation (Table 3).

From the oscillatory data, two additional viscoelastic functions of interest are calculated to further extend our understanding of the ink behavior. First, the shear relaxation modulus of both inks is calculated using the approximation developed by Ninomiya and Ferry [16]

$$G(t) = G'(\omega) - 0.4G''(0.4\omega) + 0.014G''(10\omega) \quad (4)$$

where  $\omega$  is the angular frequency ( $\omega = 1/t$ ). The results of this analysis are shown in Figure 8. The fugitive organic ink is significantly stiffer than the reference ink over the time scales examined and its relaxation is delayed. To more clearly illustrate this behavior, the relaxation spectrum is computed for each ink using Alfrey's approximation [9]

$$H(t) \approx -\left[\frac{dG(t)}{d \ln t}\right] \quad (5)$$

and the results are included in Figure 8. The fugitive ink features a single relaxation peak centered at  $10^0$  s that extends over 6 decades (based on half-height width) while the commercial ink shows a peak relaxation centered at  $10^{-6}$  s and a narrower distribution ( $\sim 3$  decades). This significant shift in relaxation to longer timescales enables more stable ink structures at ambient conditions post-deposition.

#### 4 STRUCTURAL BEHAVIOR OF FUGITIVE INK FILAMENTS

During direct-write assembly of 3D microvascular networks, the organic ink must maintain its cylindrical filamentary shape and support itself even as it spans gaps in the underlying layers. With knowledge of the ink's viscoelastic properties, we develop a structural model of the time dependent deformation of a spanning filament and compare this to experimental observations of filament deflection across a gap of varying distances.

The ink filament can be modeled using beam mechanics. Based on known solutions for the quasi-static form of Euler-Bernoulli beam theory, we write an expression for the time-dependent mid-span deflection,  $w$ , of a filament by invoking the correspondence principle such that [17]

$$w(t) = \frac{CqL^4}{384I} D(t) \quad (6)$$

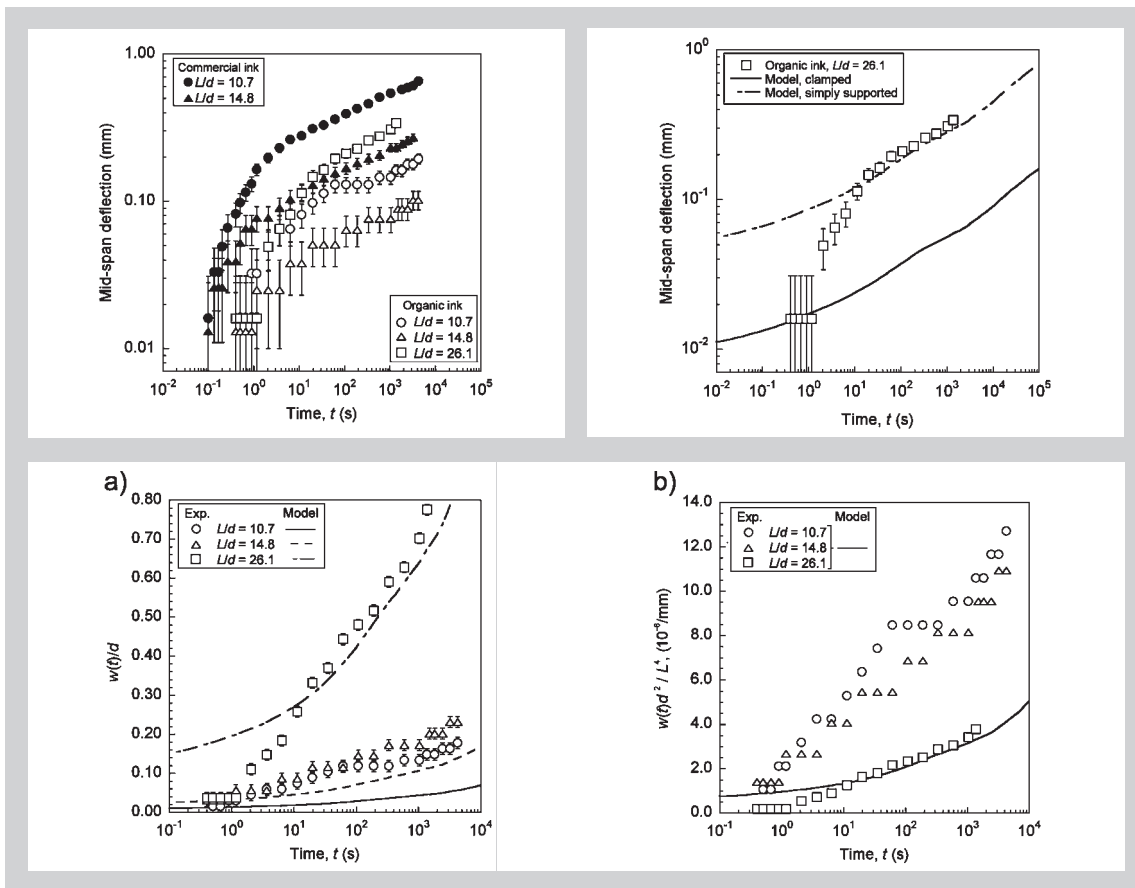


Figure 9 (left above): Self-supporting ink filament experimental results for organic and commercial inks at  $T = 20^\circ\text{C}$ .

Figure 10 (right above): Experimental data and structural model predictions using clamped and simply supported boundary conditions for organic ink ( $L/d = 26.1$ ),  $T = 20^\circ\text{C}$ .

Figure 11 (below): Normalized mid-span deflection of organic ink self-supporting filament and structural model predictions using simply supported boundary conditions,  $T = 20^\circ\text{C}$ .

a) Normalization:  $w(t)/d$ .  
b) Normalization:  $w(t)d^2/L^4$ .

where  $q$  is a uniformly distributed line load,  $L$  is the filament length,  $I$  is the moment of inertia,  $D(t)$  is the tensile creep compliance, and  $C$  is a constant equal to 1 or 5 for clamped and simply supported boundary conditions, respectively. If the filament cross-section is constant then  $q = \rho g A$  where  $\rho$  is the ink density,  $g$  is the acceleration of gravity, and  $A$  is the cross-sectional area.

To apply Eq. 6 for the inks studied, the rheological data must be recast in terms of the tensile creep compliance,  $D(t)$ . For this purpose, the complex shear compliance,  $J^*$ , can be obtained by direct inversion of the complex shear modulus, i.e.  $J^* = G^{*-1}$ . The transient shear creep compliance can then be approximated by the method of Ninomiya and Ferry [16] where

$$J(t) = J'(\omega) + 0.4J''(0.4\omega) - 0.014J''(10\omega) \quad (7)$$

which requires  $J'$  at the corresponding frequency  $\omega = 1/t$  and  $J''$  at two other frequencies. Relating the tensile and shear creep compliances yields,

$$D(t) = \frac{J(t)}{2(1+\nu)} \quad (8)$$

where Poisson's ratio,  $\nu$ , is assumed to be constant and equal to 0.5. This assumption is reasonable considering that the inks are soft viscoelastic solids tested at temperatures well

above their  $T_g$  ( $\sim -60^\circ\text{C}$ ) and the experimental timescale probed during the filament deflection experiments are relatively long.

The experimental mid-span deflection data for filaments of both organic and commercial inks over a range of different aspect ratios are plotted as a function of time in Figure 9. The organic ink filaments exhibit considerably less deformation over the entire timescale of the experiment, as compared to the commercial ink. In both cases, the rate of deformation is initially high and then begins to slow and stabilize after approximately 1 s. For both inks, the 1.07-mm filament tests ( $L/d = 10.7$ ) yielded the largest deformation compared to the 0.44 mm filament tests ( $L/d = 14.8, 26.1$ ) since the distributed weight of the filament scales with the square of the filament diameter.

Structural model predictions for mid-span deflection using Eq. 6 and  $D(t)$  from rheological data for both clamped ( $C = 1$ ) and simply supported ( $C = 5$ ) boundary conditions are shown in Figure 10 together with the experimental data for the organic ink for  $L/d = 26.1$ . Both forms of the structural model exhibit nearly constant log-log deflection rates with significantly smaller deflections predicted for the clamped boundary case. Good correlation to the experimental data is achieved at extended time for the simply supported boundary case and analysis of experimental images indicates rotation of the filament

cross-section occurs at the support, consistent with the structural behaviour of simply supported beams.

The mid-span deflection measurements are normalized by the filament diameter and shown alongside the corresponding normalized structural model predictions for the fugitive organic ink in Figure 11a. For the range of aspect ratios investigated, the model predictions are slightly lower than the experimental data for extended time periods where the maximum observed deviation was ~ 10% after 1 h for the case  $L/d = 10.7$ . At short times (i.e.  $t < 10$  s) only the predictions for the highest aspect ratio case (i.e.  $L/d = 26.1$ ) exceed the measured values since the predicted deflection rate is quite high. For further insight into the spanning behavior of an ink filament, the mid-span deflection  $w(t)$  was normalized so that geometric and material effects are isolated such that,

$$\frac{w(t)d^2}{L^4} = KD(t) \quad (9)$$

and  $K$  is a constant. Thus, the model predictions for the three aspect ratios investigated collapse onto a single curve since the material property  $D(t)$  is assumed identical. The normalized experimental data are shown in Figure 11b together with the model prediction. In this case excellent correlation is obtained for the slender beam ( $L/d = 26.1$ ) although significant deviations at long times are observed for the short beam cases. The deviation between the experimental data and the model predictions for  $L/d = 10.7$  and  $14.8$  is likely a result of structural model limitations. First and foremost, the quasi-static solution of the Euler-Bernoulli beam theory is not recommended for short beams ( $L/d < 20$ ) since the additional deformation due to the transverse shear is not considered. Additionally, material properties were obtained by rheological experiments under low amplitude shear and are restricted to the linear viscoelastic regime. However, within the nozzle, the ink yields under high shear in the region near the wall ( $\tau > \tau_y^{app}$ ) leading to a sharp decrease in the material stiffness followed by a period of recovery as the ink exits the nozzle. The deformation occurring during the yielding and recovery periods at short times were difficult to observe due to the spatial and time resolutions of

the experimental setup used. Other contributing factors such as slumping of the ink cross-section [18] and axial tension in the self-supporting filament [19] may limit the model's application. Developing a more complex structural model without these limitations and numerical simulations by finite element method are expected to provide more accurate deformation predictions at extended time periods for a wider range of filament aspect ratios.

## 5 CONCLUSIONS

A fugitive organic ink has been developed that shows superior rheological properties compared to a commercial ink used in the direct-write assembly of microvascular networks. A blend of 60wt% low molecular weight paraffin wax and 40wt% high molecular weight microcrystalline wax yields an ink system that extrudes easily at room temperature yet retains structural shape post-deposition. The new organic ink has higher stiffness (about one order of magnitude) across the entire spectrum of applied frequency together with a relatively modest apparent yield stress (1.0 kPa). More importantly, the new organic ink displays a relaxation spectrum centered at 1 s, a shift of 6 decades longer in time compared to the commercial ink. Thus, network structures deposited using the new organic ink are much more stable and persistent. For example, for an aspect ratio ( $L/d$ ) of 14.8 the total deflection after one hour is less than 20% of the filament diameter for the organic ink compared to about 65% for the commercial ink system. A structural model using Euler-Bernoulli viscoelastic beam mechanics provides good predictive capability for slender ( $L/d > 20$ ) beams and reasonable correlation for filaments with moderate length ( $10 < L/d < 20$ ). Further refinements in process modeling are needed to characterize the ink flow inside the deposition nozzle and the structural recovery immediately after deposition. These analyses will provide important information for the design of future fugitive inks and help define the processing parameters. High-performance inks combined with accurate process modeling of the direct-write assembly technique will enable the creation of microvascular networks with unparalleled complexity and commercialization of technological applications in biomedical, advanced materials and microfluidics.

## ACKNOWLEDGMENTS

The authors acknowledge funding for this project provided by AFOSR Aerospace and Materials Science Directorate (Grant # F49620-03-1-0179), U.S. Department of Energy, Division of Materials Science under Award# DEFG02-91ER45439 through the Frederick Seitz Materials Research Laboratory (UIUC), and the NSF Center for Directed Assembly of Nanostructures (Grant # DMR-01-177792). The robotic deposition apparatus used in this work was designed and built by J. Cesarano and the customized software for the 3D fabrication was developed by J.E. Smay. Partial support for D. Therriault was provided by the University of Illinois Nanoscience and Technology Center Fellowship and the government of Québec (NATEQ).

## REFERENCES

- [1] Ziaie B et al.: Hard and Soft Micromachining for BioMEMS: Review of Techniques and Examples of Applications in Microfluidics and Drug Delivery, *Adv. Drug Delivery Rev.* 56 (2004) 145-172.
- [2] Losey MW et al.: Microfabricated Multiphase Packed-Bed Reactors: Characterization of Mass Transfer and Reactions, *Ind. Eng. Chem. Res.* 40 (2001) 2555-2562.
- [3] Walker GM et al.: Cell Infection within a Microfluidic Device using Virus Gradients, *Sens. Actuators B* 98 (2004) 347-355.
- [4] White S et al.: Autonomic Healing of Polymer Composites, *Nature* 409 (2001) 794-797.
- [5] Therriault D et al.: Chaotic Mixing in Three-Dimensional Microvascular Networks Fabricated by Direct-Write Assembly, *Nature Mater.* 2 (2003) 265-271.
- [6] Lewis JA, Gratson GM: Direct Writing in Three Dimensions, *Mater. Today* 7 (2004) 32-39.
- [7] Therriault D et al.: Fugitive Inks for Direct-Write Assembly of Three-Dimensional Microvascular Networks, *Adv. Mater.* 17 (2005) 395-399.
- [8] Cesarano J et al.: Robocasting Provides Moldless Fabrication from Slurry Deposition, *Ceram. Ind.* 148 (1998) 94-102.
- [9] Ward IM, Hadley DW: *An Introduction to the Mechanical Properties of Solid Polymers*, J. Wiley and Sons, New York (1993).
- [10] Wunderlich B: *Thermal analysis*, Academic Press Inc., New York (1990).
- [11] Rueb CJ, Zukoski CF: Viscoelastic Properties of Colloidal Gels, *J. Rheol.* 41 (1997) 197-218.
- [12] Therriault D: Ph.D. dissertation, Department of Aerospace Engineering, University of Illinois at Urbana-Champaign (2003).
- [13] Carreau PJ et al.: *Rheology of Polymeric Systems, Principles and Applications*, Hanser, Cincinnati (1997).
- [14] Vega JF et al.: Model Linear Metallocene-Catalyzed Polyolefins: Melt Rheological Behavior and Molecular Dynamics, *J. Rheol.* 47 (2003) 1505-1521.
- [15] Polacco G et al.: Dynamic Master Curves of Polymer Modified Asphalt from Three Different Geometries, *Appl. Rheol.* 13 (2000) 118-124.
- [16] Ferry JD: *Viscoelastic Properties of Polymers*, J. Wiley and Sons, New York (1980).
- [17] Chen TM: The Hybrid Laplace Transform/Finite Element Method Applied to the Quasi-Static and Dynamic Analysis of Viscoelastic Timoshenko Beams, *Int. J. Numer. Methods Eng.* 38 (1995) 509-522.
- [18] Smay JE et al.: Colloidal Inks for Directed Assembly of 3-D Periodic Structures, *Langmuir* 18 (2002) 5429-5437.
- [19] Morissette SL et al.: Solid Freeform Fabrication of Aqueous Alumina-Poly(vinyl alcohol), *J. Am. Ceram. Soc.* 83 (2000) 2409-2417.

